



## Scalable synthesis of ultrathin MoS<sub>2</sub> membranes for dye desalination

Rodrigo Schneider <sup>a,b,c</sup>, Ameya Manoj Tandel <sup>c</sup>, Erda Deng <sup>c</sup>, Daniel S. Correa <sup>a,b,\*</sup>, Haiqing Lin <sup>c,\*</sup>

<sup>a</sup> Nanotechnology National Laboratory for Agriculture (LNNA), 13560-970, São Carlos, São Paulo, Brazil

<sup>b</sup> PPGQ, Department of Chemistry, Center for Exact Sciences and Technology, Federal University of São Carlos (UFSCar), 13565-905, São Carlos, São Paulo, Brazil

<sup>c</sup> Department of Chemical and Biological Engineering, University at Buffalo, The State University of New York, 14260, Buffalo, NY, USA



### ARTICLE INFO

**Keywords:**  
MoS<sub>2</sub>  
Membranes  
Dye desalination  
Hydrothermal reaction  
Ultrasonic exfoliation

### ABSTRACT

Molybdenum disulfide (MoS<sub>2</sub>) has been fabricated into thin-film composite (TFC) membranes for dye desalination due to its excellent underwater stability and tunable interlayer spacing. However, it remains challenging to synthesize thin layers of MoS<sub>2</sub> with high water permeance and high dye rejection due to the difficulty in fabricating large crystalline sheets or exfoliation. Herein, we report a scalable method coupling bottom-up hydrothermal synthesis and top-down ultrasonic exfoliation to obtain well-dispersed MoS<sub>2</sub> nanosheets and a vacuum filtration method to prepare ultrathin membranes (thickness: 30–60 nm) for dye desalination. The MoS<sub>2</sub> nanosheets and membranes are thoroughly characterized for their chemistries and nanostructures. The membrane with 60-nm MoS<sub>2</sub> exhibits water permeance of 32 LMH/bar, Na<sub>2</sub>SO<sub>4</sub> rejection of 2.3%, and Direct Red-80 rejection of 99.0%. The MoS<sub>2</sub> membranes exhibit dye desalination performance superior to state-of-the-art commercial polyamide membranes and many leading membranes based on two-dimensional materials.

### 1. Introduction

Textile dyeing and finishing is one of the most chemically intensive industries and the largest industrial polluter of clean water. The wastewater contains a significant number of toxic dyes with a detrimental impact on the environment and salts with high osmotic pressure (Chen et al., 2022; Lin et al., 2016; Shinde et al., 2021). State-of-the-art polyamide-based nanofiltration (NF) membranes can effectively recover dyes from the water, but they cannot separate divalent ions from the dyes and would require high pressure to overcome the osmotic pressures. Two-dimensional (2D) nanomaterials have emerged as a promising platform for constructing thin-film composite (TFC) membranes for dye desalination owing to their adjustable interlayer spacings (with a strong size-sieving ability) and large surface area for chemical functionalization (Liu et al., 2020; Yang et al., 2020).

Molybdenum disulfide (MoS<sub>2</sub>) has distinct characteristics for membrane applications, such as physical and chemical stability for underwater operation (Chu et al., 2020; Hu et al., 2023; Liu et al., 2022; Liu et al., 2020; Liu et al., 2021a, 2021b). For example, MoS<sub>2</sub> nanosheets display greater hydrophobicity and thus a lower degree of swelling by water (15%) than graphene oxides (GOs) (65%) (Chen et al., 2020; Gao et al., 2019; Ries et al., 2019). Additionally, when soaked in water for 1

day, the MoS<sub>2</sub> membrane retained the *d*-spacing at 6.2 Å, while the MXene membrane showed an increased *d*-spacing from 12.8 to 15.7 Å (Mei et al., 2022).

The key to preparing high-performance TFC membranes with 2D materials lies in the exfoliated nanosheets that can be well-dispersed in coating solutions. MoS<sub>2</sub> nanostructures can be produced using top-down or bottom-up approaches. For the top-down approaches, MoS<sub>2</sub> is intercalated using n-butyl-lithium (n-BuLi) in hexane to generate Li<sub>x</sub>MoS<sub>2</sub>, which then reacts with water to form LiOH and H<sub>2</sub> to exfoliate the nanosheets (Chen et al., 2022); the MoS<sub>2</sub> suspension can also be prepared by ultrasonic exfoliation in the liquids (Backes 2019; Ott et al., 2019). The top-down methods yield large nanosheets, but they can be time-consuming and require a large quantity of solvents or air-sensitive chemicals. For the bottom-up synthesis, the nanosheets can be obtained using a hydrothermal/solvothermal route, where sulfur and molybdenum sources react in an autoclave cell at ≈200 °C (Mphuthi et al., 2022), forming sub-micrometer particles and poorly-crystalline nanosheets (Feng et al., 2015; Wang et al., 2017; Ye et al., 2014). However, these nanosheets have a smaller amount of laminar organization, and the membranes often have very thick selective layers (25–30 μm) to achieve high dye rejection (Arshad et al., 2022).

Here we demonstrate for the first time an integration of bottom-up

\* Corresponding authors.

E-mail addresses: [daniel.correa@embrapa.br](mailto:daniel.correa@embrapa.br) (D.S. Correa), [haiqingl@buffalo.edu](mailto:haiqingl@buffalo.edu) (H. Lin).

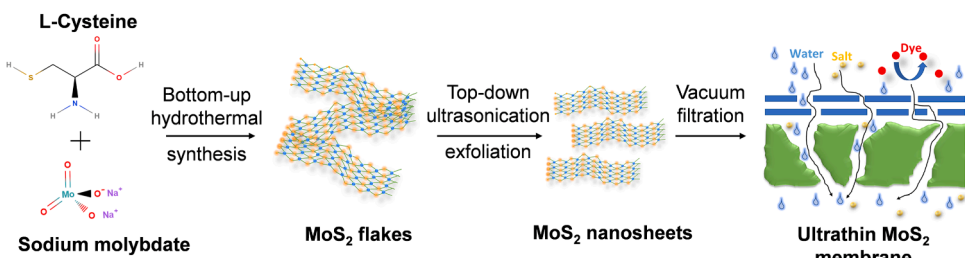


**Fig. 1.** Schematic of the scalable synthesis of MoS<sub>2</sub>-TFC membranes in three sequential steps, including bottom-up hydrothermal synthesis of MoS<sub>2</sub> flakes, top-down ultrasonic exfoliation to prepare well-dispersed nanosheets, and vacuum filtration to fabricate ultrathin membranes.

hydrothermal synthesis of large MoS<sub>2</sub> flakes and top-down ultrasonic exfoliation to obtain nanosheets large enough to prepare membranes by vacuum filtration onto polysulfone (PSF) porous support (Fig. 1). More importantly, this approach is scalable, as hydrothermal reaction and ultrasonication have been practiced for industrial material processing (Karim et al., 2023), and vacuum filtration technique has been demonstrated to fabricate 2D material-based membranes on a large scale, such as reduced GO-based membranes by roll-to-roll process (Esfahani et al.,

2023) and amine-treated GO hollow fiber membranes (Zhou et al., 2019). Our approach significantly shortens the membrane preparation time by substituting time-consuming exfoliation steps (such as n-BuLi intercalation) with 1-h ultrasonic exfoliation and does not require any additives (such as polymers or zwitterionic molecules) to create MoS<sub>2</sub> layers as thin as 30–60 nm. The nanosheets and membranes are thoroughly characterized for their chemistries and nanostructures. The MoS<sub>2</sub> membranes are evaluated for dye desalination and demonstrate the

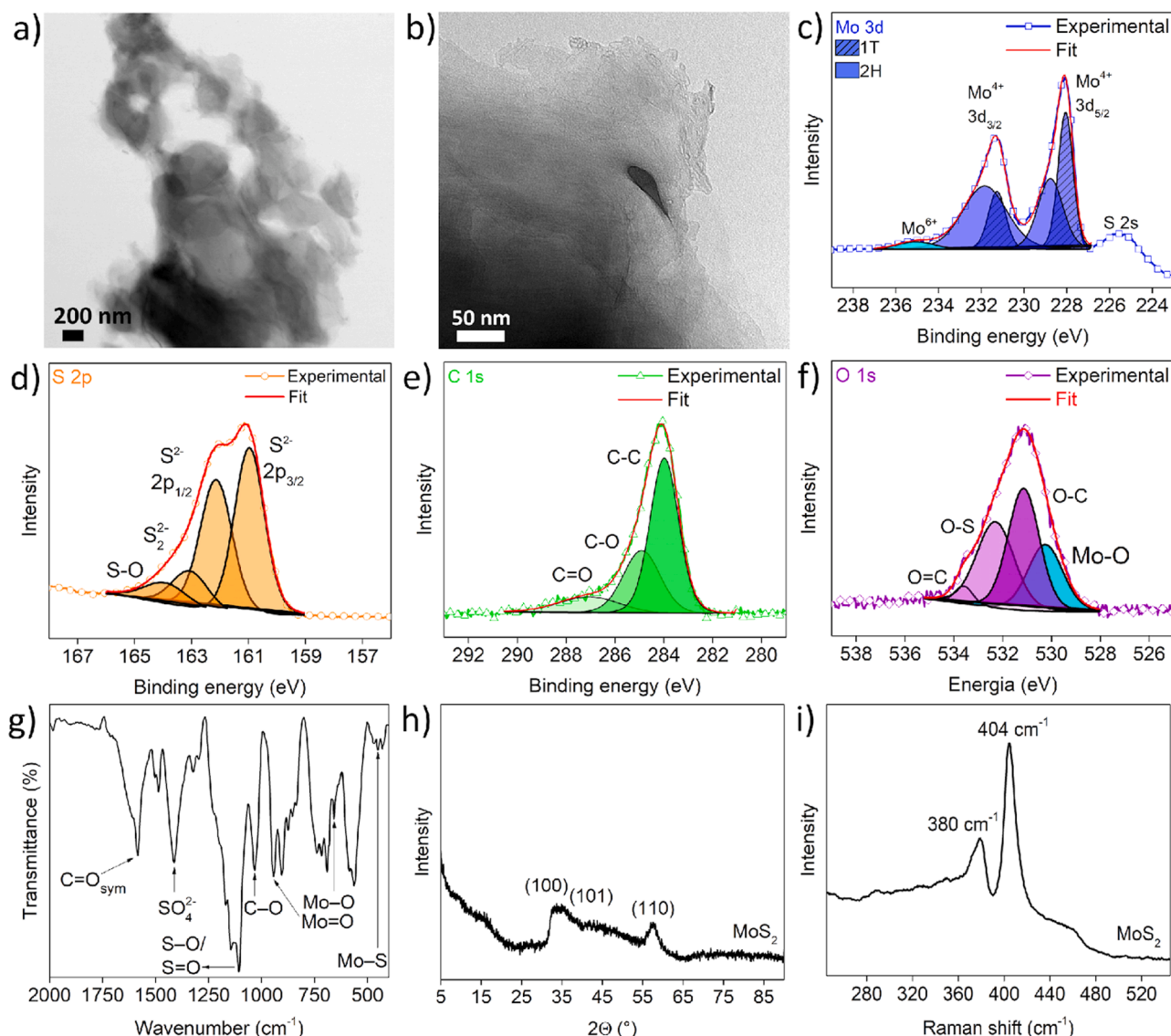


**Fig. 2.** Characterization of the MoS<sub>2</sub> flakes synthesized from L-cysteine and Na<sub>2</sub>MoO<sub>4</sub> by hydrothermal reaction. (a) TEM and (b) HRTEM images. High-resolution XPS for (c) Mo 3d region, (d) S 2p region, (e) C 1s region, and (f) O 1s region. (g) FTIR spectrum, (h) XRD pattern, and (i) Raman spectrum.

performance superior to state-of-the-art polyamide-NF membranes and other leading membranes based on 2D materials.

## 2. Experimental

### 2.1. Materials

L-Cysteine ( $C_3H_7NO_2S$ ) and sodium molybdate ( $Na_2MoO_4$ ) were purchased from Panreac and Synth (Brazil), respectively. *N,N*-Dimethylformamide (DMF), isopropyl alcohol (IPA), Direct Red 80 (DR, 1373 g/mol), Congo Red (CR, 697 g/mol), Methylene Blue (MB, 320 g/mol) and Methyl Blue (MethylB, 800 g/mol) were obtained from Sigma-Aldrich (St. Louis, MO, USA). PSF 20k support with a molecular weight cut-off of 20 kDa was provided by Solecta, Inc. (Oceanside, CA, USA).

### 2.2. Synthesis of $MoS_2$ membranes

First,  $MoS_2$  flakes were synthesized using a modified hydrothermal procedure (Schneider et al., 2021), where  $Na_2MoO_4$  (as a molybdenum source) was mixed with L-cysteine (as a sulfur source) at an Mo:S molar ratio of 2:4.5. In detail, 0.1900 g of L-cysteine and 0.2517 g of  $Na_2MoO_4$  were dissolved in 10 mL and 15 mL of water, respectively. Both solutions were mixed and heated from 25 to 200 °C at 3 °C/min in a stainless-steel autoclave. After 17-h reaction, the produced  $MoS_2$  was separated from the supernatant by centrifugation at 8000 rpm and 5 °C for 10 min and then washed with water before drying at 40 °C for 72 h to obtain black  $MoS_2$  particles.

Second, the  $MoS_2$  nanosheets were prepared by dispersing particles in DMF followed by ultrasonic exfoliation for 1 h. Third, the TFC membranes were prepared by vacuum filtration (Chen et al., 2022). Specifically, PSF support was pre-treated in IPA for 24 h and then soaked in water before the use (Tandel et al., 2022). The  $MoS_2$  suspension was diluted in water to 25 and 50 mg/L and then filtered through the support. The volume ratio of DMF to water was 5:95 and 10:90 in the solutions of 25 and 50 mg/L, respectively, and the  $MoS_2$  loading is estimated to be 15 and 30  $\mu\text{g}/\text{cm}^2$ , respectively. Finally, after the filtration, the membranes were rinsed carefully with water for 10 min and stored in water (up to 48 h) before further studies. The samples were labeled as  $MoS_2$ -15 (with an estimated  $MoS_2$  thickness of 30 nm based on its density of 5.06  $\text{g cm}^{-3}$ ) and  $MoS_2$ -30 (60 nm).

### 2.3. Characterization of $MoS_2$ nanosheets and membranes

The  $MoS_2$  flakes were characterized by Transmission Electron Microscopy (TEM, Tecnai G<sup>2</sup> F20) and Scanning Electron Microscopy (SEM, FIB-SEM, Carl Zeiss Auriga CrossBeam, Zeiss, Germany). The surface charge and Zeta potential ( $\zeta$ ) were determined by a Zetasizer NanoZS/Malvern. Fourier Transformed Infrared (FTIR) Spectroscopy with attenuated total reflectance (ATR) was employed to determine functional groups using Bruker Vertex 70. X-ray Photoelectron Spectroscopy (XPS) was performed using ESCALAB-MKII with Al K $\alpha$  (1486.6 eV) to determine the surface chemical composition. The high-resolution XPS spectra were recorded in Sulfur, Molybdenum, Carbon and Oxygen regions. Raman spectra (100–500  $\text{cm}^{-1}$ ) were obtained using HORIBA LabRAM HR Evolution. X-ray diffraction (XRD) patterns (5–70°) were obtained with a scan speed of 1°/min in an XRD-6000/Shimadzu. Dye molecular sizes were measured using dynamic light scattering (DLS) by Zetasizer Nano ZS90.

The membranes were characterized by Atomic Force Microscopy (AFM, MultiMode VIII/Bruker) for surface roughness and a Model 190 goniometer (Rame-Hart Instrument Co., Succasunna, NJ) was employed for water contact angle (WCA) measurements. For water filtration studies, the membranes were cut into coupons of 1.8 cm in diameter and tested in dead-end cells. Water permeance ( $A_W$ ,  $\text{L m}^{-2} \text{ h}^{-1} \text{ bar}^{-1}$  or LMH/bar) can be calculated using Eq. (1) (Huang et al., 2018):

$$A_W = \frac{J_W}{\Delta p} = \frac{V}{t \times \Delta p \times A_m} \quad (1)$$

where  $J_W$  is the permeate flux ( $\text{L m}^{-2}$ ),  $\Delta p$  is the transmembrane pressure (TMP, bar),  $A_m$  is the active membrane area ( $\text{m}^2$ ), and  $V$  is the volume of the water permeated (L) over the collection time  $t$  (h). The dye rejection tests were conducted with feed solutions containing 200 ppm dyes at 5 bar. The dye rejection ( $R_D$ ) is calculated using Eq. (2):

$$R_D = (1 - C_{P,D} / C_{F,D}) \times 100\% \quad (2)$$

where  $C_{P,D}$  and  $C_{F,D}$  are the dye concentration in the permeate and feed, respectively. For each membrane, at least two samples were tested, and an average value is reported.

## 3. Results and discussions

### 3.1. Synthesis and characterization of $MoS_2$ flakes and nanosheets

The successful synthesis of  $MoS_2$  flakes by bottom-up hydrothermal reaction of L-cysteine and  $Na_2MoO_4$  is confirmed by various physical and chemical characterizations. Fig. S1a shows the morphology of  $MoS_2$  nanosheets with some degree of agglomeration. Figure 2a and Fig. S1b display the TEM images of a few stacked  $MoS_2$  nanosheets with dimension of 3–5  $\mu\text{m}$ , and Fig. 2(b) shows an irregular-edged contour of nanosheets and a poorly crystalline structure, consistent with the hydrothermal  $MoS_2$  reported in the literature (Abinaya et al., 2018; Lai et al., 2021).

The high-resolution XPS data of  $MoS_2$  (Fig. 2(c)–(f)) confirm the formation of Mo-S bonds by the presence of the peaks in the Mo 3d and S 2p regions, as well as the presence of O 1s and C 1s peaks (Chen et al., 2021; Kumar et al., 2019; Lei et al., 2022). The Mo 3d region (Fig. 2(c)) demonstrates the predominance of the  $Mo^{4+}$  state centered at 228.1 eV (derived from Mo 3d<sub>5/2</sub>) and 231.4 eV (arising from Mo 3d<sub>3/2</sub>). The deconvoluted peaks indicate that hydrothermal reaction forms a mixture of 1T and 2H crystalline domains, which are assigned to the crystalline phases from 2D TMDs (Chen et al., 2021; Lee et al., 2022). The shoulder at 235.2 eV refers to the highly oxidized states of molybdenum ( $Mo^{6+}$ ), which are commonly associated with Mo-O bonds (Li et al., 2015) and can be ascribed to the atmospheric oxygen passivation, the unreacted  $Na_2MoO_4$ , or the  $MoO_3$  impurities (Lei et al., 2022; Tiwari et al., 2022). Figure 2(d) shows the two S<sup>2-</sup> oxidation states at 161.0 eV (S 2p<sub>3/2</sub>) and 162.1 eV (2p<sub>1/2</sub>). Two additional peaks are observed at 164 eV for S—O bond and at 163.2 eV for S—S bridging ( $S_2^{2-}$ ) or apical S<sup>2-</sup> (Kumar et al., 2019).

The hydrothermal reaction also introduces the O and C, forming functional groups covalently attached to or adsorbed on the  $MoS_2$  flakes. For instance, the C 1s peak is deconvoluted into three peaks for C—C (284.0 eV), C—O (285.0 eV), and C=O (287.1 eV) (Fig. 2(e)) (Kumar et al., 2019), while the O 1s peak can be deconvoluted into Mo—O (531.1 eV), C—O (231.9 eV) and C=O (233.3 eV) (Fig. 2(f)) (Liu et al., 2021a; Tang et al., 2022).

The FTIR spectrum exhibits vibrational modes from organic functionalization and confirms the surface/edge modifications or non-covalently molecules adsorbed onto the  $MoS_2$  flakes (Fig. 2(g)). The main peaks include 450  $\text{cm}^{-1}$  (Mo—S stretching (Fang et al., 2018; Zhao et al., 2020)), 658  $\text{cm}^{-1}$  (Mo—O (Tang et al., 2022)), 1414  $\text{cm}^{-1}$  ( $SO_4^{2-}$  (Zhao et al., 2020)), and 1585  $\text{cm}^{-1}$  (C=O symmetric (Jiang et al., 2021)), 1107  $\text{cm}^{-1}$  ( $SO_3$  (Singh et al., 2022)), and 943/905  $\text{cm}^{-1}$  (Mo=O (Tang et al., 2022; Zhao et al., 2020)). These peaks also corroborate with the XPS analysis. The functional groups are expected to increase the  $d$ -spacing due to the steric hindrance between basal planes of the nanosheets and the reduced van der Walls stacking along the z-axis. Additionally, the  $MoS_2$  shows a negative zeta potential value of  $\zeta = -28.8 \pm 1.6$  mV, consistent with the literature (Schneider et al., 2021).

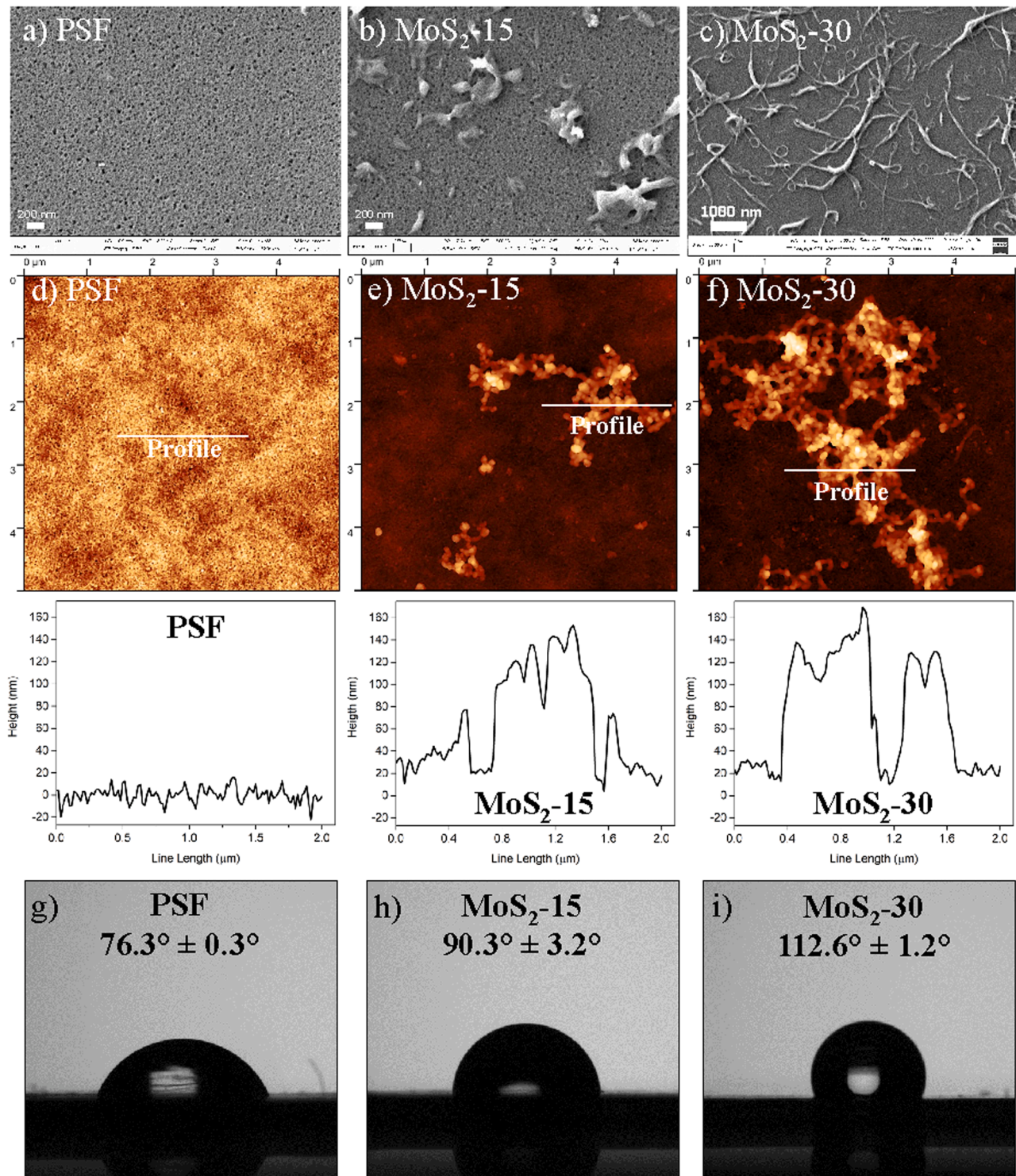


**Fig. 3.** Surface characterization of the PSF and MoS<sub>2</sub> membranes. (a–c) SEM images of membrane surfaces. (d–f) AFM 2D images and topological height variation profile. (g–i) Water contact angles.

Figure 2(h) displays the XRD pattern of MoS<sub>2</sub> with low-intensity and broad peaks, suggesting a non-crystalline structure, which is typical for those prepared by the hydrothermal route (Abinaya et al., 2018; Ye et al., 2014). The (100) plane is assigned to S-terminated edge (Posysaev and Alatalo, 2019), (101) refers to basal plane facets (An et al., 2022), and (110) peak at  $2\theta = 58.3^\circ$  refers to the distance between Mo and S in the sheets. Interestingly, the characteristic peak at  $2\theta \approx 14.5^\circ$  (*d*-spacing of  $\approx 6.2$  Å) associated with stacking of MoS<sub>2</sub> flakes (002 plane) is not

present in the diffractogram, probably due to their nanomorphology (Fig. 2(a)). Figure 2(i) displays the Raman spectrum with the two characteristic peaks of MoS<sub>2</sub> structures of  $404\text{ cm}^{-1}$  ( $A_{1g}$ ) and  $380\text{ cm}^{-1}$  ( $E_{2g}^1$ ).

### 3.2. Characterization of the MoS<sub>2</sub> membranes

Figure 3(a)–(c) displays the SEM images of the pristine PSF, MoS<sub>2</sub>–

**Table 1**

Comparison of water permeance and dye rejection in PSF, MoS<sub>2</sub>-15, and MoS<sub>2</sub>-30. DR, CR, and MethylB have negative surface charges, and MB has a positive charge.

Membranes	MWCO (kDa)	DR solution $A_W$ (LMH/bar)	Dye rejection (%)			
			DR (-)	CR (-)	MethylB (-)	MB (+)
PSF	31	750 ± 120	79	78	16	8
MoS <sub>2</sub> -15	36	200 ± 40	91	91	38	12
MoS <sub>2</sub> -30	36	32 ± 6	99	91	60	9

15, and MoS<sub>2</sub>-30, respectively. The PSF shows a porous surface with an average pore size of 20–30 nm. The deposition of 25 mg/L MoS<sub>2</sub> solution results in agglomerates on the surface, which is not fully covered, reaching a MoS<sub>2</sub> loading of 15 µg/cm<sup>2</sup>, similar to those reported in the literature (Abinaya et al., 2018). By contrast, the deposition of 50 mg/L MoS<sub>2</sub> appears to completely cover the surface and forms wrinkles, reaching a loading of 30 µg/cm<sup>2</sup>, which are characteristics of 2D nanosheets (Huang et al., 2018). The SEM cross-section images for the MoS<sub>2</sub> membranes were obtained (Fig. S2), but the thickness of the MoS<sub>2</sub> layer is too low to be determined using the collected SEM image. Fig. S3a–c also confirms that the deposition of thin MoS<sub>2</sub> layers does not change the appearance of the membrane surface.

The AFM images of the membranes (Fig. 3(d)–(f)) show the well-defined pores on the PSF membrane and the MoS<sub>2</sub> deposition, consistent with the SEM images (Fig. 3(a)–(c)). The pristine PSF displays a smooth surface with an average roughness ( $R_a$ ) of 8.3 nm. Increasing the MoS<sub>2</sub> content in the suspensions increases the  $R_a$  values. For example, MoS<sub>2</sub>-15 and MoS<sub>2</sub>-30 show the  $R_a$  values of 21 and 37 nm, respectively.

Figure 3(a)–(I) compares the static WCAs for various membranes. PSF support shows the WCA of 76.3 ± 0.3°. The MoS<sub>2</sub> deposition increases the WCA, indicating the enhanced hydrophobicity. MoS<sub>2</sub>-30 exhibits greater hydrophobicity than MoS<sub>2</sub>-15 because of the higher coverage and thicker MoS<sub>2</sub> layer (Gao et al., 2016; Tran et al., 2020).

### 3.3. MoS<sub>2</sub> membrane for water purification

Table 1 compares steady-state dye solution permeance ( $A_W$ ) and dye rejection for PSF and MoS<sub>2</sub> membranes. As expected, increasing the MoS<sub>2</sub> thickness decreases the dye solution permeance, though all membranes show similar values of molecular weight cut-off (MWCO)

(Fig. S4). Nevertheless, MoS<sub>2</sub>-15 exhibits water permeance of 200 LMH/bar, much higher than those observed for polyamide-based NF membranes.

PSF support shows higher rejection to the dyes with negative charges (such as DR and CR) than MB with a positive charge because of the negative charge on the membrane surface (Dashtbozorg et al., 2022; Gholami et al., 2022). On the other hand, MethylB exhibits rejection lower than expected (though it has molecular weight similar to CR), presumably because MethylB has smaller aggregates than CR in aqueous solutions. Positively charged dyes can be easily adsorbed by the negatively charged membranes, while the negatively charged dyes might be excluded by the Donnan effect (Deng et al., 2017; Ding et al., 2022; Fang et al., 2022; Liu et al., 2021a).

The MoS<sub>2</sub> membranes exhibit much higher dye rejection than PSF support (despite similar MWCOs), especially for the negatively charged DR and CR. For example, MoS<sub>2</sub>-30 exhibits DR rejection of 99% (much higher than 79% in PSF) and CR rejection of 91% (higher than 78% in PSF), and the reduced DR concentration in the permeate can be viewed by the color difference from the feed solution (Fig. S5). The superior separation properties of MoS<sub>2</sub> membranes can be partially ascribed to their suitable interlayer spacings and hydrophobicity, rendering robust underwater molecular sieving abilities. However, the MoS<sub>2</sub> layers are too thin to be characterized using x-ray diffraction for the  $d$ -spacing. On the other hand, the positively charged MB exhibits low rejection in the MoS<sub>2</sub> membranes because of the negative charge of the MoS<sub>2</sub>. Fig. S3 also compares the surface color change after the DR test for the three membranes. The MoS<sub>2</sub> layer deposition reduced the DR adhesion, indicating the improved antifouling properties. Additionally, all membranes show very low rejection of NaCl and MgCl<sub>2</sub> (~3%).

Table 2 compares the developed MoS<sub>2</sub> membranes with those reported in the literature (which were often derived from n-BuLi exfoliation). Our approach avoids the use of additives or long-time intercalation processes, and it does not require any additional surface coating to eliminate defects (Gao et al., 2019; Li et al., 2018), which would lower water permeance. The strategy of employing bottom-up route to synthesize MoS<sub>2</sub> particles combined with a top-down ultrasonic exfoliation in DMF renders well-dispersed MoS<sub>2</sub> nanosheets for facile fabrication of membranes using scalable vacuum filtration. More importantly, our MoS<sub>2</sub> selective layers have the thickness of 30–60 nm, much thinner than others reported in the literature, while achieving good desalination performance of negatively charged dyes.

**Table 2**

Comparison of the dye removal performance of our MoS<sub>2</sub> TFC membranes with those reported in the literature, as well as synthesis routes, thickness, and porous supports.

MoS <sub>2</sub> synthesis	Thickness (nm)	MoS <sub>2</sub> modification	Porous support	Dyes or ions	Rejection (%)	$A_W$ (LMH/ bar)	Ref.
Top-down (n-BuLi)	250	Acetamide-; methyl-; ethyl-2-ol-MoS <sub>2</sub>	Nylon	Phtalocyanine	100	>3	(Ries et al., 2019)
	500	–	PES	Pb <sup>2+</sup>	–	145	(Wang et al., 2020)
	1700	–	PTFE	Evans blue (+)	90.3	245	(Sun et al., 2013)
	462	–	PVDF	MB (+)	82	25	(Lu et al., 2020)
Top-down (ultrasonic exfoliation)	4540	PSBMA <sup>†1</sup> /PDA	HPAN	MB (+)	99.8	108	(Zhang et al., 2021)
	100	β-CD and TDI <sup>†2</sup>	PVP	CR (–)	95	30	(Feng et al., 2022)
	4500	O-MoS <sub>2</sub> <sup>†3</sup>	PES	Rose Bengal (–)	99.9 99.6	75 55	(Tian et al., 2023)
	80	TA-MoS <sub>2</sub> <sup>†4</sup>	PES	CR (–)	99.6	55	(Fan et al., 2018)
Bottom-up	–	PTCA <sup>†5</sup>	PES	CR (–)	79	217	(Sreeramareddy et al., 2021)
Hydrothermal synthesis & ultrasonic exfoliation	30–60		PSF	CR (–) DR (–)	91 99	32	This work

<sup>†1</sup> Poly(sulfobetaine methacrylate).

<sup>†2</sup> β-Cyclodextrin and toluene-2,4-diisocyanate.

<sup>†3</sup> Molybdenum disulfide oxide.

<sup>†4</sup> Tannic acid.

<sup>†5</sup> Polythiocyanuric.

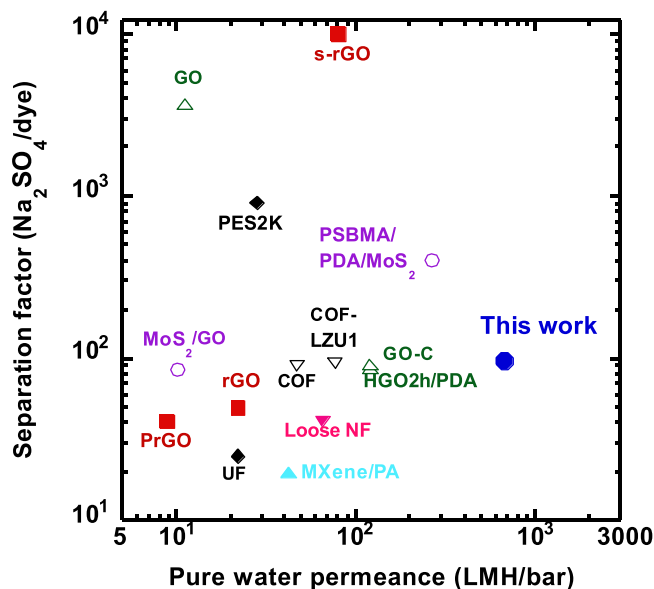


**Fig. 4.** Comparison of the  $\text{MoS}_2$  membranes with state-of-the-art membranes for dye/ $\text{Na}_2\text{SO}_4$  separation. The data are also summarized in Table S2.

Nevertheless, in this study, the membranes were often stored in water for up to 48 h, and the permeation tests often last for 2 h due to the high water flux of these membranes. Consequently, their long-term stability for continuous permeation tests needs to be validated.

The separation factor ( $\alpha$ ) of the salt over dye is defined as:

$$\alpha = (1 - R_s)/(1 - R_d) \quad (3)$$

where  $R_s$  is the rejection of the salt. Figure 4 compares the separation factor of our  $\text{MoS}_2$  membranes with state-of-the-art membranes for dye desalination. The  $\text{MoS}_2$ -30 membrane shows a good water permeance and separation factor comparable with other membranes based on  $\text{MoS}_2$  (Zhang et al., 2021; Zhang et al., 2019), COF (Fan et al., 2018; Shinde et al., 2021), rGO (Han et al., 2013; Zhu et al., 2017) and MXene (Wang et al., 2022). Other 2D materials-based TFC membranes like GOs (Chen et al., 2018) and S-rGO (Huang et al., 2018) exhibit higher separation factor but lower water permeance than our  $\text{MoS}_2$  membranes.

#### 4. Conclusions

We demonstrate a facile fabrication of ultrathin membranes by vacuum filtration of  $\text{MoS}_2$  nanosheets, which were synthesized using an integrated approach of bottom-up hydrothermal reaction in aqueous solutions and top-down ultrasonic exfoliation in DMF. This approach yields large, well-dispersed nanosheets, which exhibit negative charges and remarkable hydrophobicity. TFC membranes containing  $\text{MoS}_2$  selective layers of 30–60 nm were successfully prepared and demonstrate desalination performance of negatively charged dyes superior to state-of-the-art commercial NF membranes and many 2D materials-based membranes.

#### CRediT authorship contribution statement

**Rodrigo Schneider:** Conceptualization, Data curation, Investigation, Writing – original draft. **Ameya Manoj Tandel:** Data curation, Writing – review & editing. **Erda Deng:** Data curation, Writing – review & editing. **Daniel S. Correa:** Conceptualization, Writing – review & editing, Supervision. **Haiqing Lin:** Conceptualization, Supervision, Writing – review & editing.

#### Declaration of Competing Interest

The authors declare that they have no known competing financial interests or personal relationships that could have appeared to influence the work reported in this paper.

#### Data availability

Data will be made available on request.

#### Acknowledgments

The authors thank the financial support from Fundação de Amparo à Pesquisa do Estado de São Paulo (FAPESP) (Grants 2018/18468-2 and 2018/22214-6), Conselho Nacional de Desenvolvimento Científico e Tecnológico (CNPq), MCTI-SisNano (CNPq/402.287/2013-4), and Coordenação de Aperfeiçoamento de Pessoal de Nível Superior - Brasil (CAPES) – Código de Financiamento 001, CAPES/PrINT no. 88887.569937/2020-00 - Edital n. 41/2017 and Rede Agronano-EMBRAPA from Brazil. We also thank the Laboratory of Structural Characterization (LCE/DEMa/UFSCar) for the microscopy facilities and SEM images, and to the Brazilian Nanotechnology National Laboratory (LNNano/CNPEM) for the AFM images. Also, we would like to thank Dr. Marcelo Barbosa de Andrade from the Centro de Caracterização de Espécies Minerais (CCEM-IFSC) for allowing access to the micro-FT-Raman facilities and measurements. AT, ED, and HL also acknowledge support from the Department of Energy Office of Energy Efficiency and Renewable Energy (DE-EE0009500).

#### Supplementary materials

Supplementary material associated with this article can be found, in the online version, at doi:10.1016/j.memlet.2023.100058.

#### References

- Abinaya, R., Archana, J., Harish, S., Navaneethan, M., Ponnusamy, S., Muthamizhchelvan, C., Shimomura, M., Hayakawa, Y., 2018. Ultrathin layered  $\text{MoS}_2$  nanosheets with rich active sites for enhanced visible light photocatalytic activity. *RSC Adv.* 8 (47), 26664–26675.
- An, C.-H., Kang, W., Deng, Q.-B., Hu, N., 2022. Pt and Te codoped ultrathin  $\text{MoS}_2$  nanosheets for enhanced hydrogen evolution reaction with wide pH range. *Rare Metals* 41 (2), 378–384.
- Arshad, F., Aubry, C., Zou, L., 2022. Highly permeable  $\text{MoS}_2$  nanosheet porous membrane for organic matter removal. *ACS Omega* 7 (2), 2419–2428.
- Backes, C., 2019. Ten years of liquid-phase exfoliation of layered crystals—A bright future ahead? *Chimia (Aarau)* 73, 498.
- Chen, H., He, X., Zhou, Z., Wu, Z., Li, H., Peng, X., Zhou, Y., Tan, C., Shen, J., 2022. Metallic phase enabling  $\text{MoS}_2$  nanosheets as an efficient sonosensitizer for photothermal-enhanced sonodynamic antibacterial therapy. *J. Nanobiotechnol.* 20 (1), 136.
- Chen, L., Moon, J.-H., Ma, X., Zhang, L., Chen, Q., Chen, L., Peng, R., Si, P., Feng, J., Li, Y., Lou, J., Ci, L., 2018. High performance graphene oxide nanofiltration membrane prepared by electrospraying for wastewater purification. *Carbon* 130, 487–494.
- Chen, X., Bartlam, C., Lloret, V., Badlyan, N.M., Wolff, S., Gillen, R., Stimpel-Lindner, T., Maultzsch, J., Duesberg, G.S., Knirsch, K.C., Hirsch, A., 2021. Covalent bisfunctionalization of two-dimensional molybdenum disulfide. *Angew. Chem. Int. Ed.* 60 (24), 13484–13492.
- Chen, X., Feng, Z., Gohil, J., Stafford, C.M., Dai, N., Huang, L., Lin, H., 2020. Reduced holey graphene oxide membranes for desalination with improved water permeance. *ACS Appl. Mater. Interfaces* 12 (1), 1387–1394.
- Chu, C., Fu, C.-F., Zhang, P., Pan, T., Ai, X., Wu, Y., Cui, P., Huang, Q., Ran, J., 2020. Precise angstrom controlling the interlayer channel of  $\text{MoS}_2$  membranes by cation intercalation. *J. Membr. Sci.* 615, 118520.
- Dashtbozorg, A., Saljoughi, E., Mousavi, S.M., Kiani, S., 2022. High-performance and robust polysulfone nanocomposite membrane containing 2D functionalized MXene nanosheets for the nanofiltration of salt and dye solutions. *Desalination* 527, 115600.
- Deng, M., Kwac, K., Li, M., Jung, Y., Park, H., 2017. Stability, molecular sieving, and ion diffusion selectivity of a lamellar membrane from two-dimensional molybdenum disulfide. *Nano Lett.* 17 (4), 2342–2348.

- Ding, H., Xie, F., Wang, Z., Huang, W., Ma, X., Xu, Z., 2022. 2D nanosheets optimized electrospray-assisted interfacial polymerization polyamide membrane with excellent separation performance. *J. Membr. Sci.* 647, 120308.
- Esfahani, A.R., Ma, C., Flewellen, U.A., Nair, S., Harris, T.A.L., 2023. Scalable aqueous-phase fabrication of reduced graphene oxide nanofiltration membranes by an integrated roll-to-roll (R2R) process. *J. Membr. Sci.* 678, 121669.
- Fan, H., Gu, J., Meng, H., Knebel, A., Caro, J., 2018. High-flux membranes based on the covalent organic framework COF-LZU1 for selective dye separation by nanofiltration. *Angew. Chem. Int. Ed.* 57 (15), 4083–4087.
- Fang, S., Gong, J., Tang, L., Cao, W., Li, J., Tan, Z., Niu, Q., Chen, Z., 2022. Construction the hierarchical architecture of molybdenum disulfide/MOF composite membrane via electrostatic self-assembly strategy for efficient molecular separation. *Chem. Eng. J.* 449, 137808.
- Fang, Y., Huang, Q., Liu, P., Shi, J., Xu, G., 2018. A facile dip-coating method for the preparation of separable MoS<sub>2</sub> sponges and their high-efficient adsorption behaviors of Rhodamine B. *Inorg. Chem. Front.* 5 (4), 827–834.
- Feng, W., Chen, L., Qin, M., Zhou, X., Zhang, Q., Miao, Y., Qiu, K., Zhang, Y., He, C., 2015. Flower-like PEGylated MoS<sub>2</sub> nanoflakes for near-infrared photothermal cancer therapy. *Sci. Rep.* 5 (1), 17422.
- Gao, J., Zhang, M., Wang, J., Liu, G., Liu, H., Jiang, Y., 2019. Bioinspired modification of layer-stacked molybdenum disulfide (MoS<sub>2</sub>) membranes for enhanced nanofiltration performance. *ACS Omega* 4 (2), 4012–4022.
- Feng, Y., Meng, X., Zhang, Z., Zhang, L., 2022. Dye retention and desalination behavior of MoS<sub>2</sub> doped high-flux PCP/TDI polyurethane nanofiltration membrane. *J. Membr. Sci.* 656, 120643.
- Gao, X., Wang, X., Ouyang, X., Wen, C., 2016. Flexible superhydrophobic and superoleophilic MoS<sub>2</sub> sponge for highly efficient oil-water separation. *Sci. Rep.* 6 (1), 27207.
- Gholami, F., Asadi, A., Zinatizadeh, A.A., 2022. Efficient heavy metals and salts rejection using a novel modified polysulfone nanofiltration membrane. *Appl. Water Sci.* 12 (7), 146.
- Han, Y., Xu, Z., Gao, C., 2013. Ultrathin graphene nanofiltration membrane for water purification. *Adv. Funct. Mater.* 23 (29), 3693–3700.
- Hu, C., Achari, A., Rowe, P., Xiao, H., Suran, S., Li, Z., Huang, K., Chi, C., Cherian, C.T., Sreepal, V., Bentley, P.D., Pratt, A., Zhang, N., Novoselov, K.S., Michaelides, A., Nair, R.R., 2023. pH-dependent water permeability switching and its memory in MoS<sub>2</sub> membranes. *Nature* 616 (7958), 719–723.
- Huang, L., Huang, S., Venka, S.R., Lin, H., 2018. Rightsizing nanochannels in reduced graphene oxide membranes by solvating for dye desalination. *Environ. Sci. Technol.* 52 (21), 12649–12655.
- Jiang, Y., Wang, J., Wu, J., Zhang, Y., 2021. Preparation of high-performance natural rubber/carbon black/molybdenum disulfide composite by using the premixture of epoxidized natural rubber and cysteine-modified molybdenum disulfide. *Polym. Bull.* 78 (3), 1213–1230.
- Karim, S.S., Sudais, A., Shah, M.S., Farrukh, S., Ali, S., Ahmed, M., Salahuddin, Z., Fan, X., 2023. A contemplating review on different synthesis methods of 2D-Molybdenum disulfide (MoS<sub>2</sub>) nanosheets. *Fuel* 351, 128923.
- Kumar, N., Fosso-Kankeu, E., Ray, S.S., 2019. Achieving controllable mos<sub>2</sub> nanostructures with increased interlayer spacing for efficient removal of Pb(II) from aquatic systems. *ACS Appl. Mater. Interfaces* 11 (21), 19141–19155.
- Lai, M., Lee, K., Yang, T.C.K., Pan, G., Lai, C., Chen, C., Johan, M.R., Juan, J., 2021. The improved photocatalytic activity of highly expanded MoS<sub>2</sub> under visible light emitting diodes. *Nanoscale Adv.* 3 (4), 1106–1120.
- Lee, J., Lin, M., Wu, J., 2022. High-efficiency cycling piezo-degradation of organic pollutants over three liters using MoS<sub>2</sub>/carbon fiber piezocatalytic filter. *Nano Energy* 98, 107280.
- Lei, R., Gao, F., Yuan, J., Jiang, C., Fu, X., Feng, W., Liu, P., 2022. Free layer-dependent piezoelectricity of oxygen-doped MoS<sub>2</sub> for the enhanced piezocatalytic hydrogen evolution from pure water. *Appl. Surf. Sci.* 576, 151851.
- Li, M., Sun, X., Wang, L., Wang, S., Afzal, M.Z., Song, C., Wang, S., 2018. Forward osmosis membranes modified with laminar MoS<sub>2</sub> nanosheet to improve desalination performance and antifouling properties. *Desalination* 436, 107–113.
- Li, X., Li, X., Zang, X., Zhu, M., He, Y., Wang, K., Xie, D., Zhu, H., 2015. Role of hydrogen in the chemical vapor deposition growth of MoS<sub>2</sub> atomic layers. *Nanoscale* 7 (18), 8398–8404.
- Lin, J., Ye, W., Baltaru, M.C., Tang, Y., Bernstein, N.J., Gao, P., Balta, S., Vlad, M., Volodin, A., Sotto, A., Luis, P., Zydny, A.L., Van der Bruggen, B., 2016. Tight ultrafiltration membranes for enhanced separation of dyes and Na<sub>2</sub>SO<sub>4</sub> during textile wastewater treatment. *J. Membr. Sci.* 514, 217–228.
- Liu, Y., Li, X., Liu, T., Zheng, Z., Liu, Q., Wang, Y., Qin, Z., Guo, H., Liang, Y., 2022. Alcohols assisted in-situ growth of MoS<sub>2</sub> membrane on tubular ceramic substrate for nanofiltration. *J. Membr. Sci.* 659.
- Liu, Y., Qin, Z., Zhang, X., Wang, N., Liu, T., Cui, S., An, Q., Guo, H., 2021a. In-situ growth of graphene quantum dots modified MoS<sub>2</sub> membrane on tubular ceramic substrate with high permeability for both water and organic solvent. *J. Membr. Sci.* 627, 119247.
- Liu, Y., Zhang, X., Zhao, Y., 2020. Two-dimensional mos<sub>2</sub> nanomaterials and applications in water treatment. *Prog. Chem.* 32 (5), 642–655.
- Liu, Y., Zhao, Y., Zhang, X., Huang, X., Liao, W., Zhao, Y., 2021b. MoS<sub>2</sub>-based membranes in water treatment and purification. *Chem. Eng. J.* 422, 130082.
- Lu, X., Gabinet, U.R., Ritt, C.L., Feng, X., Deshmukh, A., Kawabata, K., Kaneda, M., Hashmi, S.M., Osuji, C.O., Elimelech, M., 2020. Relating selectivity and separation performance of lamellar two-dimensional molybdenum disulfide (MoS<sub>2</sub>) membranes to nanosheet stacking behavior. *Environ. Sci. Technol.* 54 (15), 9640–9651.
- Mei, L., Cao, Z., Ying, T., Yang, R., Peng, H., Wang, G., Zheng, L., Chen, Y., Tang, C.Y., Voiry, D., Wang, H., Farimani, A.B., Zeng, Z., 2022. Simultaneous electrochemical exfoliation and covalent functionalization of MoS<sub>2</sub> membrane for ion sieving. *Adv. Mater.* 34 (26), 2201416.
- Mphuthi, N., Sikhwiwihlu, L., Ray, S.S., 2022. Functionalization of 2D MoS<sub>2</sub> nanosheets with various metal and metal oxide nanostructures: their properties and application in electrochemical sensors. *Biosensors* 12 (6), 386.
- Ott, S., Wolff, N., Rashvand, F., Rao, V.J., Zaumseil, J., Backes, C., 2019. Impact of the MoS<sub>2</sub> starting material on the dispersion quality and quantity after liquid phase exfoliation. *Chem. Mater.* 31 (20), 8424–8431.
- Posysaev, S., Alatalo, M., 2019. Surface morphology and sulfur reduction pathways of MoS<sub>2</sub> Mo edges of the monolayer and (100) and (103) surfaces by molecular hydrogen: a DFT study. *ACS Omega* 4 (2), 4023–4028.
- Ries, L., Petit, E., Michel, T., Diogo, C.C., Gervais, C., Salameh, C., Bechelany, M., Balme, S., Miele, P., Onofrio, N., Voiry, D., 2019. Enhanced sieving from exfoliated MoS<sub>2</sub> membranes via covalent functionalization. *Nat. Mater.* 18 (10), 1112–1117.
- Schneider, R., Facure, M.H.M., Alvarenga, A.D., Chagas, P.A.M., dos Santos, D.M., Correa, D.S., 2021. Dye adsorption capacity of MoS<sub>2</sub> nanoflakes immobilized on poly (lactic acid) fibrous membranes. *ACS Appl. Nano Mater.* 4 (5), 4881–4894.
- Shinde, D.B., Cao, L., Liu, X., Wonanke, D.A.D., Zhou, Z., Hedhili, M.N., Addicoat, M., Huang, K.-W., Lai, Z., 2021. Tailored pore size and microporosity of covalent organic framework (COF) membranes for improved molecular separation. *J. Membr. Sci.* Lett. 1 (2), 100008.
- Singh, V.K., Jain, P., Panda, S., Kuila, B.K., Pitchaimuthu, S., Das, S., 2022. Sulfonic acid/sulfur trioxide (SO<sub>3</sub>H/SO<sub>3</sub>) functionalized two-dimensional MoS<sub>2</sub> nanosheets for high-performance photocatalysis of organic pollutants. *New J. Chem.* 46 (28), 13636–13642.
- Sreeramareddygari, M., Mannekote Shivanna, J., Somasundrum, M., Soontarapa, K., Surareungchai, W., 2021. Polythiocyanuric acid-functionalized MoS<sub>2</sub> nanosheet-based high flux membranes for removal of toxic heavy metal ions and congo red. *Chem. Eng. J.* 425, 130592.
- Sun, L., Huang, H., Peng, X., 2013. Laminar MoS<sub>2</sub> membranes for molecule separation. *Chem. Comm.* 49 (91), 10718–10720.
- Tandel, A.M., Rawda, N., Deng, E., Lin, H., 2022. Ultrathin-film composite (uTFC) membranes based on amorphous perfluoropolymers for liquid separations. *J. Membr. Sci.* 663, 121015.
- Tang, D., Li, J., Yang, Z., Jiang, X., Huang, L., Guo, X., Li, Y., Zhu, J., Sun, X., 2022. Fabrication and mechanism exploration of oxygen-incorporated 1T-MoS<sub>2</sub> with high adsorption performance on methylene blue. *Chem. Eng. J.* 428, 130954.
- Tian, H., Yang, S., Wu, X., Zhang, K., 2023. Two-dimensional molybdenum disulfide oxide (O-MoS<sub>2</sub>) enhanced tight ultrafiltration membrane with improved molecular separation performance and antifouling properties. *Colloids Surf. A: Physicochem. Eng.* 656, 130328.
- Tiwari, P., Jaiswal, J., Chandra, R., 2022. Optical and electrical tunability in vertically aligned MoS<sub>2</sub> thin films prepared by DC sputtering: role of film thickness. *Vacuum* 198, 110903.
- Tran, T., Tu, Y.-C., Hall-Laureano, S., Lin, C., Kawy, M., Lin, H., 2020. Nonstick membranes prepared by facile surface fluorination for water purification. *Ind. Eng. Chem. Res.* 59 (12), 5307–5314.
- Wang, Y., Sunarso, J., Wang, F., Zhao, B., Liu, X., Chen, G., 2017. Electrospinning and hydrothermal synthesis of recyclable MoS<sub>2</sub>/CNFs hybrid with enhanced visible-light photocatalytic performance. *Ceram. Int.* 43 (14), 11028–11033.
- Wang, Z., Tu, Q., Sim, A., Yu, J., Duan, Y., Poon, S., Liu, B., Han, Q., Urban, J.J., Sedlak, D., Mi, B., 2020. Superselective removal of lead from water by two-dimensional MoS<sub>2</sub> nanosheets and layer-stacked membranes. *Environ. Sci. Technol.* 54 (19), 12602–12611.
- Wang, Y., Xu, H., Ding, M., Zhang, L., Chen, G., Fu, J., Wang, A., Chen, J., Liu, B., Yang, W., 2022. MXene-regulation polyamide membrane featuring with bubble-like nodule for efficient dye/salt separation and antifouling performance. *RSC Adv* 12 (17), 10267–10279.
- Yang, S., Jiang, Q., Zhang, K., 2020. Few-layers 2D O-MoS<sub>2</sub> TFN nanofiltration membranes for future desalination. *J. Membr. Sci.* 604.
- Ye, L., Xu, H., Zhang, D., Chen, S., 2014. Synthesis of bilayer MoS<sub>2</sub> nanosheets by a facile hydrothermal method and their methyl orange adsorption capacity. *Mater. Res. Bull.* 55, 221–228.
- Zhang, M., Gao, J., Liu, G., Zhang, M., Liu, H., Zhou, L., Liu, Y., Zheng, X., Jiang, Y., 2021. High-throughput zwitterion-modified MoS<sub>2</sub> membranes: preparation and application in dye desalination. *Langmuir* 37 (1), 417–427.
- Zhang, P., Gong, J.-L., Zeng, G.-M., Song, B., Cao, W., Liu, H.-Y., Huan, S.-Y., Peng, P., 2019. Novel “loose” GO/MoS<sub>2</sub> composites membranes with enhanced permeability for effective salts and dyes rejection at low pressure. *J. Membr. Sci.* 574, 112–123.
- Zhao, M., Ma, X., Yan, S., Xiao, H., Li, Y., Hu, T., Zheng, Z., Jia, J., Wu, H., 2020. Solvothermal synthesis of oxygen-incorporated MoS<sub>2-x</sub> nanosheets with abundant undercoordinated Mo for efficient hydrogen evolution. *Int. J. Hydrog. Energy* 45 (38), 19133–19143.
- Zhou, F., Tien, H.N., Dong, Q., Xu, W.L., Li, H., Li, S., Yu, M., 2019. Ultrathin, ethylenediamine-functionalized graphene oxide membranes on hollow fibers for CO<sub>2</sub> capture. *J. Membr. Sci.* 573, 184–191.
- Zhu, L., Wang, H., Bai, J., Liu, J., Zhang, Y., 2017. A porous graphene composite membrane intercalated by halloysite nanotubes for efficient dye desalination. *Desalination* 420, 145–157.